Electric Power Systems Research 216 (2023) 109011

Contents lists available at ScienceDirect

Electric Power Systems Research

journal homepage: www.elsevier.com/locate/epsr

On the suitability of the CISPR 16 method for measuring conducted emissions in the 2–150kHz range in low voltage grids

Stefano Lodetti [a], Alexander Gallarreta [b], Deborah Ritzmann [a], Victor Khokhlov [c], Paul Wright [a], Jan Meyer [c], Igor Fernández [b], David de la Vega [b,*]

[a] National Physical Laboratory, Teddington TW11 0LW, U.K.
[b] Dpt. of Communications Engineering, University of the Basque Country (UPV/EHU), Bilbao, ES-48013, Spain
[c] Institute of Electrical Power Systems and High Voltage Engineering, Technische Universität Dresden, Dresden, 01062, Germany

ARTICLE INFO

Keywords:
Measurement methods
High frequency distortion
Power quality
Supraharmonics
Compatibility levels

ABSTRACT

The IEC 61000–2–2 standard defines the compatibility levels to evaluate the conducted disturbances in the low voltage grid for the 2-150 kHz range. For frequencies 9–150 kHz, they are defined in terms of quasi peak values measured according to CISPR 16–1–1 standard, but no clear guidance is given on how to apply this standard to grid measurements. The definition of the method in CISPR 16–1–1 accepts a wide range of different implementations, all of them fulfilling the compliance requirements. The reasons are that the standard does not propose a fixed implementation but a 'black-box' approach, and some of the proposed configuration values are non-normative and/or wide tolerances are allowed. In this context, some parameters have a pivotal role in the results provided by the method. The impact of variation of these parameters on the measurement results is addressed in this work. In particular, the accuracy requirements and the reproducibility issues of the standard are studied. For that purpose, a high number of different compliant implementations have been developed and the influence of different features of the CISPR 16–1–1 method on the results of these implementations is identified and analyzed. The results show that the wide tolerances allowed by the CISPR 16 specification impede the comparison of results provided by measuring receivers based on different implementations of the standard. Results of the study also show that reproducibility issues for the same input signal may be relevant and generate inconsistences. Moreover, a fixed specific configuration does not ensure that uncertainty issues are solved, as the technical approach used in the implementation of the damped meter has a strong influence on the outputs. An unambiguous guidance of digital implementation of the standard could fix these issues.

1. Introduction

In the last decade, increasing levels of conducted interference and disturbances have been observed in low voltage (LV) power grids in the frequency range 2 kHz to 150 kHz (supraharmonics). Although it could be expected that distortions in this frequency range could be of lower amplitude than harmonics of the fundamental frequency, this can potentially change in the near future because they are mainly due to the increasing penetration of renewable energy sources (RESs) connected to the grid via power electronic converters, electric vehicles (EVs), and extensive use of communication technologies in the grid e.g., power line communication (PLC) [1–4]. Distortion in the 2 kHz to 150 kHz region has been reported to cause additional heating in electronic devices which reduces their lifetime, acoustic noise from equipment, malfunction and increased failure rate of equipment, wrong meters reading, and failed operation of grid devices [1,5–7],. Moreover, high-amplitude emissions in this range may disturb PLC performance and even isolate PLC devices during some intervals [7,8], and therefore, a comprehensive evaluation of their effect on power quality and PLC performance is pending to determine their relevance. The addition of filters is not always possible, as they would also filter the PLC transmissions out.

While this is already recognized as cause for concern, with the increasing penetration of RESs and inverter-connected devices in the grid, the risk of interference in this frequency region is expected to increase. For this reason, it is essential to carefully monitor this phenomenon by accurately measuring the levels of disturbance and providing useful power quality (PQ) indices. While considerable effort is

* Corresponding author.
E-mail address: david.delavega@ehu.eus (D. de la Vega).

https://doi.org/10.1016/j.epsr.2022.109011
Received 7 June 2022; Received in revised form 20 October 2022; Accepted 19 November 2022
Available online 30 November 2022

being put towards establishing a consistent standardization framework, at the moment this frequency range lacks a normative measurement method for LV networks. Such method is required to ensure comparability and accuracy of measurement, and to secure electromagnetic compatibility (EMC) against increasing level of disturbances in the 2 kHz to 150 kHz range. Methods to quantify conducted emissions in the LV grid in the frequency range 2 kHz to 150 kHz are currently under study, and in the last few years new methods have been proposed in the literature. Recent works have focused on comparative analysis between new and existing measurement methods in this frequency range. Extensive comparisons can be found in [9–11]. The ongoing research work is providing valuable knowledge to standardization bodies, which are actively working towards addressing the gaps in the normative and regulatory framework in the supraharmonic range, including the IEC SC77A which is responsible for the IEC 61000–4–30. Meanwhile, some non-normative methods are reported in the IEC 61000-4-30 Annex C [12]: for frequencies 2 kHz to 9 kHz, the method described in the IEC 61000–4–7 Annex B [13], while for 9 kHz to 150 kHz, three tentative methods are considered. First, the adoption of IEC 61000–4–7 Annex B [13] up to 150 kHz is proposed, which may require some modifications to adapt the time windowing and the frequency resolution to the 9 kHz to 150 kHz range, still to be determined. The second proposal is a lighter method, with the use of gaps and considering a lower frequency resolution in order to reduce the computational and storage requirements for PQ instruments [12]. Finally, the CISPR 16–1–1 method [14] [15], is the only proposed method based on a quasi-peak (QP) detector of 200 Hz bandwidth to assess the amplitude values of disturbances, and therefore, the only method that allows the comparison of the disturbances against the compatibility levels stated in the IEC 61000–2–2 standard [16], which are defined in terms of QP values for the 9 kHz to 150 kHz range. This aspect represents a valuable benefit with respect to the other two methods. However, the IEC 61000–4–30 standard itself raises concerns about this method, because it is designed for laboratory and may not be optimized for in-situ measurements. It is complex and expensive to be implemented, due to gapless and accuracy requirements [12]. A further serious concern is the black-box approach of the CISPR 16-1-1 standard and the lack of a unique reference implementation of the method. In combination with high tolerances of up to ±3.5 dB (+50% / −33%), different compliant implementations are possible, which may not satisfy the reproducibility requirements usually applied to grid measurements e.g., ±5% for harmonic measurements below 2 kHz [13]. Therefore, a serious question about the suitability of the CISPR 16 standard as a reference method for field measurements of disturbances in LV power grids arises.

In order to address this question, this paper studies the accuracy requirements and the reproducibility of the CISPR 16–1–1 measurement method. For this purpose, a high number of compliant implementations of this standard are thoroughly analyzed and the sources of divergence of the results are identified. The paper is structured as follows: an overview of the CISPR 16–1–1 measurement method is presented in Section 2; the accuracy requirements of this method are analyzed in Section 3, while the reproducibility issues are studied in Section 4, based on the outputs of a high number of compliant implementations for two test waveforms recorded in the LV electrical grid. A discussion of the outcomes and further analysis are described in Section 5, and Section 6 summarizes the conclusions of this work.

2. Overview of the CISPR 16 measurement method

The CISPR 16 standard specifies instrument characteristics [14] and methods [15] for measuring radio disturbance and immunity in the frequency range 9 kHz to 18 GHz. For historical reasons, the instrument characteristics are based on analogue super-heterodyne electromagnetic interference (EMI) receivers that sequentially scan the frequency range to detect worst-case appliance emissions. A block diagram of an EMI receiver is shown in Fig. 1. The input voltage signal is first processed by a pre-selector and attenuator to increase dynamic range and control the input amplitude to the mixer and local oscillator, which down-convert the signal to an intermediate frequency [14]. The signal is then band pass filtered with a frequency response within the mask specified in CISPR 16–1–1. Finally, the signal envelope is processed by a detector of choice (average, rms-average, peak or QP).

The sequential scan is a time-consuming operation and does not allow for simultaneous gapless measurements in time and frequency. For this reason, new instruments using digital technology have been developed and are recognized as compliant if performance requirements defined by CISPR 16 are met [17],[18]. CISPR 16 Part 3 gives background information on the definition of such digital instruments [19]. The main stages of a digital implementation are illustrated schematically in Fig. 2. After digitization, the input voltage signal is decomposed into frequency components using a spectral analysis tool, usually the short-time Fourier transform (STFT), resulting in a time-dependent frequency spectrum [17]-[19]. The time series of amplitude values per frequency are processed by digital simulation of the CISPR 16 detectors; in this work, the interest is on the QP detector, which is used to compare the results to the compatibility levels in the range 2 kHz to 150 kHz [16].

An analogue QP detector consists of an RC circuit and a critically damped meter as shown in Fig. 3. The behavior of these analogue components can be simulated digitally by a cascade of infinite impulse response (IIR) filters [20]. The QP detector weights the envelope of each frequency component; then, the maximum of the weighted envelope gives the final measurement value. The QP detector was originally

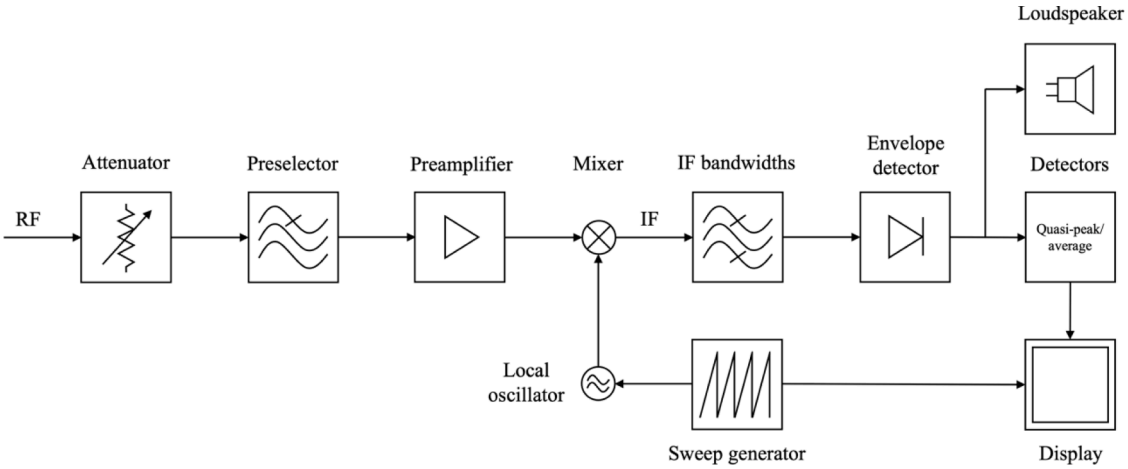

Fig. 1. Block diagram of an EMI receiver, according to CISPR 16–1–1 standard [14].

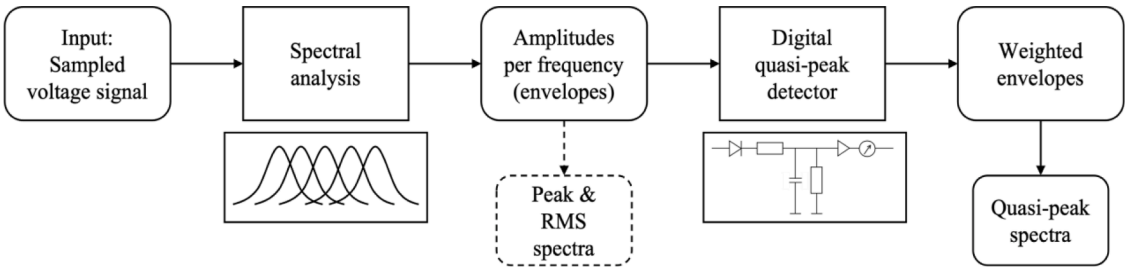

Fig. 2. Diagram of the digital implementation of a CISPR 16–1–1 receiver.

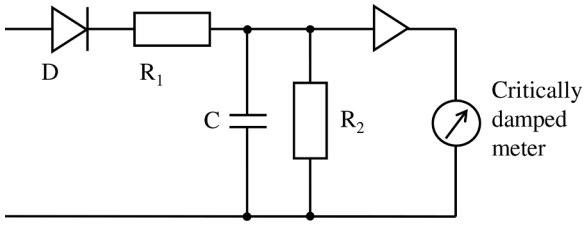

Fig. 3. Scheme of a QP detector, according to CISPR 16–1–1 standard.

developed to evaluate the annoyance to the human ear of a repetitive disturbance. As a result, disturbances with high repetition rates are weighted to provide higher QP values.

CISPR 16 does not provide normative specifications for the parameters of the STFT, but the window function must be chosen such that each frequency component complies with the reference bandwidth and selectivity mask, and the overlap of consecutive windows must be high enough to measure short pulses accurately. Non-normative Annex H of CISPR 16–1–1 specifies values for the time constants of the RC circuit and critically damped meter of the QP detector, but different values are allowed as long as the instrument meets the performance requirements.

3. Accuracy requirements of the CISPR 16–1–1 method

This section illustrates the accuracy requirements of the CISPR 16 measurement algorithm and discusses how they compare with the accuracy requirements that are normally employed for in-situ PQ measurements.

Firstly, the standard allows wide tolerances for the time constants that characterize the QP measuring receiver. The Annex H of the standard lists constant values for defining the performance of the RC circuit (charging and discharging time), the response of the critically damped meter (mechanical time) and overload factors [14]. However, these time constants are not normative, so they are not mandatory for a compliant implementation of the QP detector. Moreover, the Annex D (normative) of the standard allows a tolerance value of 20% for these time constants, considering the influence of the analog receiver characteristics upon its pulse response [14].

Secondly, the CISPR 16–1–1 measurement method is defined with a black-box approach i.e. no specific circuit topology design is prescribed but the compliance is determined based on passing a series of tests defined in the normative Annex K of the standard. From the point of view of accuracy, the relevant compliance tests are the overall pass-band selectivity, the sine-wave voltage tolerance, and the response to pulses [14].

The overall pass-band selectivity compliance test specifies the selectivity that the frequency decomposition stage should provide. The CISPR 16–1–1 standard defines a frequency mask and states that the overall selectivity of the measuring receiver shall lie within the limits of the mask, as it is shown in Fig. 4. For analogue super-heterodyne receivers, this corresponds to the frequency response of the band pass filter (see Fig. 1); in modern digital Fourier transform (DFT)-based measuring

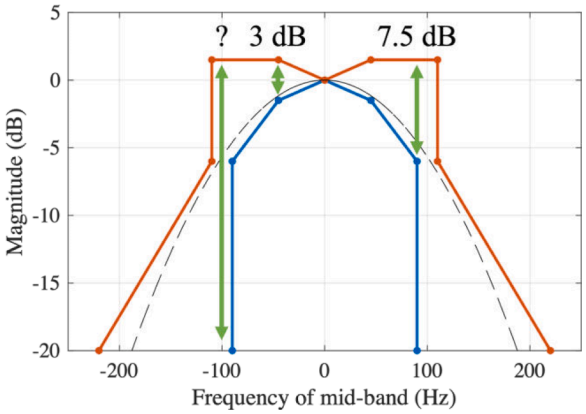

Fig. 4. CISPR 16–1–1 pass-band selectivity mask, adapted from [14], delimited by upper (red) and lower (blue) boundaries. The black dashed line represents an example of a compliant frequency response.

instruments, the frequency selectivity is determined by the weighting window of the STFT, whose frequency response must fit into the mask shown in Fig. 4. The frequency mask has a -6 dB width of approximately 200 Hz, and a unit gain at the center of the pass-band. However, apart from these two constraints, the limits for the selectivity mask are defined with wide tolerances. Hence, at ± 50 Hz from the center of the band, the defined tolerance is 3 dB, while at ± 90 Hz the tolerance is 7.5 dB and indeterminate at ± 100 Hz. These relaxed requirements are related to the analogue definition of the method some decades ago, as old analogue filters had a much lower precision compared to modern digital filter implementations. Therefore, a large variability in the selectivity is permitted, and many different windows are compliant with the overall pass-band selectivity and can be considered in the implementation of the measuring receiver.

The second compliance test, i.e. the sine-wave voltage tolerance, requires an accuracy of ± 2 dB when measuring a pure sine-wave signal, using a 50 Ω resistive source impedance [14]. This should be tested individually for start, stop and center frequencies of the CISPR bands, which for CISPR Band A means 9 kHz, 79.5 kHz and 150 kHz. This compliance test is similar to the accuracy test for harmonic measurements (below 2 kHz) where the IEC 61000–4–7 standard requires an accuracy of $\pm 5\%$ for single-frequency and steady-state signals [13]. The CISPR 16–1–1 target accuracy for pure sine-waves, however, is much more permissive, since ± 2 dB corresponds to $+26\%$ / -21%.

The third compliance test defined by the standard focuses on the response to a sequence of pulses of specific pulse repetition frequency (PRF). When the input signal is a train of pulses with a defined pulse area of 13.5 μVs and a PRF of 25 Hz, the output spectrum should be uniform up to 150 kHz (for CISPR Band A) with an amplitude equal to the response to an unmodulated sine-wave signal at the tuned frequency having an electromotive force (EMF) of 2 mV_{rms} [14]. Since there is a well-defined reference value for the amplitude, this compliance test is called absolute calibration. The tolerance for this requirement is ± 1.5

dB. In addition, compliance is assessed for other six values of PRF. These tests are considered a relative calibration because their reference level is given relative to the amplitude level obtained with the absolute test at PRF = 25 Hz (see Table 1 for expected amplitude levels and tolerances for every PRF). For instance, when measuring a pulse train at PRF = 10 Hz, the output of the measuring instrument should be

$$x_{10\ Hz} = x_{25\ Hz} + (4 \pm 1)\ dB \quad (1)$$

where $x_{25\ Hz}$ is the response to an unmodulated sine-wave signal at the tuned frequency having an EMF of 2 mV_{rms}. However, considering that $x_{25\ Hz}$ already has a tolerance of ±1.5 dB with respect to the nominal amplitude x_0, the overall tolerance becomes

$$x_{10\ Hz} = (x_0 \pm 1.5)\ dB + (4 \pm 1)\ dB = ((x_0 + 4) \pm 2.5)\ dB \quad (2)$$

Therefore, the accumulated tolerance (see Table 1) allowed by this compliance test for a PRF of 10 Hz is ±2.5 dB, i.e. +33% / - 25%. The greatest tolerance margins of this compliance test are for PRF values of 1 Hz and 2 Hz: ±3.5 dB, i.e. +50% / −33%.

In summary, the requirements for compliance with CISPR 16–1–1 (up to +50% / −33%.) are significantly higher than the values that are normally employed for PQ measurements below 2 kHz (±5%).

In addition, CISPR 16–1–1 does not define the temporal shape of the pulses used in the calibration process. It only states the pulse area and the specifications in the frequency domain for these signals. Annex K of CISPR 16–1–1 allows the use of manufacturer's calibration processes or the test performed in calibration laboratories, provided that the specification described in standard are met [14]. Therefore, the temporal behavior of the test signals can be chosen by the user, which leads to different calibration results [21]. Thus, the ambiguity in the definition of the test signals in conjunction with the large tolerances allowed in the calibration results in a wide range of compliant CISPR 16–1–1 implementations [22].

It should be noted that Annex A in CISPR 16–1–1 specifies the frequency response that an analogue compliant receiver should fulfill, only for a waveform in the form of a train of periodically repeated pulses. This definition is not a specific implementation of the CISPR 16 method, but a black-box approach that delimits the behavior to a specific input test waveform, which does not ensure that different implementations provide the same output, even more to inputs different from a pulse train. Moreover, the translation of this response based on analogue circuitry into digital processing techniques is neither unique nor obvious. This generates that different implementations of the method, all of them fulfilling the requirements of the standard, provide a wide range of outputs for the same input signal. The following section investigates the dispersion of the outputs with respect to the accuracy requirements usually applied to LV grid measurements.

4. Reproducibility between different CISPR 16–1–1 implementations

The black-box approach (Section 0), together with the wide tolerances allowed for compliance (Section 0), lead to a wide range of different compliant implementations of the method described in CISPR 16–1–1. These implementations generate different results for the same input waveform, which may cause reproducibility issues.

In this section, the variety of implementations that can be obtained is explored, investigating its impact on the reproducibility of the measurement results. Being the most widely employed approach, the analysis focuses on digital DFT-based CISPR 16–1–1 implementations, although other processing techniques are also allowed by the standards.

4.1. Methodology

The characteristics of an DFT-based CISPR 16–1–1 method are mainly determined by (i) the STFT weighting window, (ii) the overlap factor of the STFT, and (iii) the implementation of the QP detector. Therefore, the analysis of reproducibility developed in this work is focused on these three characteristics.

In this work, by varying these parameters, different implementations of the CISPR 16–1–1 method were obtained; in particular, 15 different weighting windows, 11 different overlap factors, and 3 different QP digital implementations were considered, which gives a total of 495 different combinations. However, the performance with respect to the compliance tests was evaluated and 26.3% of these combinations did not pass the compliance tests described in Section 3. Therefore, a total of 365 compliant implementations were obtained.

In the following, the choices of the parameters are briefly discussed and then, the obtained CISPR 16–1–1 implementations are applied to two different types of input waveforms, in order to evaluate the reproducibility of the results.

4.2. Parameters

The spectral analysis, based on the STFT, is dependent on the type of weighting window used in the implementation [23]. Many types of windows fulfill the mask stated by the standard for the frequency selectivity (discussed in Section 3) and, therefore, all of them are candidates for the STFT weighting window. The parameters of the 15 windows considered in this study are outlined in Table 2. Among them, the first 11 windows were specifically designed for this work, selected among the most widely used families, while windows 12 to 15 were taken from the literature. In particular, the Gaussian window ID 15 was taken from CISPR/TR 16–3, which is not normative [19], and the Lanczos kernel window ID 13 was selected because its main lobe most closely matches the spectral response for the pre-receiver described in Annex A of CISPR 16–1–1 [14],[24]. All the tested windows have a length of 20 ms, for obtaining a frequency step size of 50 Hz, as it is proposed in CISPR/TR 16–3 [19]. As it can be seen in Fig. 5, all of them are compliant with the frequency selectivity mask.

Another crucial parameter of the STFT is the overlap factor between consecutive weighting windows in the time domain [23]. On the one

Table 1
Pulse response of quasi-peak measuring receivers.

PRF (Hz)	Difference from reference amplitude (dB)	Tolerance (dB)	Accumulated tolerance (dB)
100	–4	±1	±2.5
60	–3	±1	±2.5
25	0 (ref.)		±1.5
10	+4	±1	±2.5
5	+7.5	±1.5	±3
2	+13	±2	±3.5
1	+17	±2	±3.5

Table 2
Tested weighting windows.

ID	Family	Parameters
1	Gaussian	α = 5
2	Gaussian	α = 5.3
3	Gaussian [25]	α = 5.8
4	Generalized Normal	α = 3.5, p = 4
5	Generalized Normal	α = 4.2, p = 4
6	Generalized Normal	α = 3.6, p = 6
7	Generalized Normal	α = 3.3, p = 6
8	Generalized Normal	α = 3.9, p = 6
9	Kaiser	β = 23
10	Kaiser	β = 28
11	Kaiser	β = 33
12	Gaussian	α = 4.8497
13	Lanczos [24]	SLP = 1
14	Gaussian [26]	α = 5.5
15	Gaussian [19]	α = 5.34

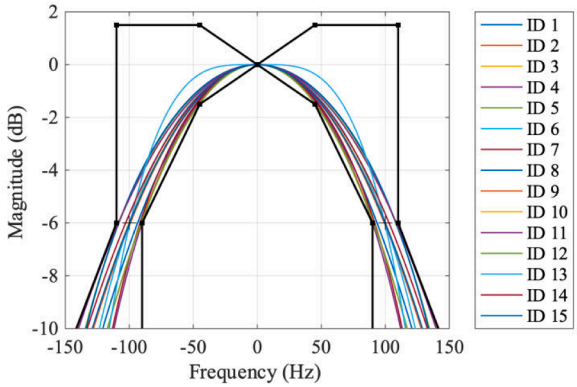

Fig. 5. Frequency response of the windows functions described in Table 2 and the frequency selectivity mask of CISPR 16–1–1 [3].

hand, low levels of overlap can lead to high errors, as they underestimate the energy of the waveform, mainly in the measurement of isolated pulses or short disturbances that occur between two consecutive windows [27,28]. For this reason, an overlap factor of at least 75% is recommended [19], and a value of 90% is highly recommended [28]. On the other hand, high levels of overlap considerably increase the computational cost of the assessment, as a higher number of Fourier transforms is needed. As a result, a trade-off of this factor should be selected in an accurate but efficient implementation. In this work, 11 values of overlap factor, from 70% to 99.5% are considered (see Table 3).

Finally, the QP detector represents another relevant variable, since its implementation can be varied freely, as long as overall compliance with the standard is fulfilled. The CISPR 16–1–1 Annex H describes the specifications of a QP measuring receiver by means of the overall characteristics, but not the specifications of the individual components [14]. They are defined in the form of time constants of the performance of the RC circuit and the critically damped meter separately. Table 4 shows the values defined for the electrical charge and discharge time constants of the RC circuit (T_C and T_D, respectively) and the mechanical time constant of the critically damped meter (T_{DM}), assuming a linear response to current for this meter, although other relations are allowed [14]. As Annex H is only informative, the fulfillment of these time constants is not normative, provided the implementation of the entire receiver passes the calibration test to be compliant with the standard. Nonetheless, Annex D (normative) indicates that, although no tolerances are defined for the time constants of the QP measuring receiver, 'it is suggested for guidance that a value of 20% is considered reasonable' [14].

Although a wide range of different implementations of the QP detector are possible, the completion of the RC circuit according to the standard is straightforward, while the critically damped meter opens the door to different approaches. Accordingly, this study has focused on different compliant implementations of the damped meter. Three compliant detectors have been developed independently resulting in minor differences in the technical approach of digital implementations from analogue specifications. In the analysis, these technical approaches have been combined with the possibility of using different time constants within a tolerance of 20% for the damped meter. This leads to the use of mechanical time constants of the damped meter of 160 ms (recommended value [14]), 128 ms (−20% tolerance) and 192 ms (+20% tolerance), for Detectors 1, 2 and 3, respectively (see Table 4). The

Table 3
Tested overlap values.

Overlap factors (%)										
70	75	80	85	90	95	96	97	98	99	99.5

Table 4
Characteristics of a Quasi-Peak Measuring Receiver [14].

	T_C (ms)	T_D (ms)	T_{DM} (ms)
Nominal	45	500	160
Detector 1	45	500	160
Detector 2	45	500	128
Detector 3	45	500	192

mechanical time constant determines the response time of the QP indicator to a change in the input values identified by the RC circuit. Therefore, a smaller time constant (Detector 2) implies a less damped implementation and, in consequence, a faster reaction of the indicator. Furthermore, a detector with a higher time constant (Detector 3) provides more damped spectra and responds more slowly to fast fluctuations of the waveforms. The effect of differences in the technical approach of the digital implementations from analogue specifications will be shown in Section 5.2.

4.3. Test waveforms

In order to evaluate the dispersion of the results provided by all the selected compliant implementations of CISPR 16–1–1, a 3-second signal recorded in the LV grid was used (see Fig. 6). The signal was recorded at a photovoltaic (PV) installation, where a PLC system was used for meter reading [25]. This recording was digitized with a sampling rate of 1 MHz and a resolution of 16 bit per sample, a quantification that provides an adequate configuration for the evaluation of LV grid distortions up to 150 kHz. This signal was selected because it contains two types of waveforms of different nature (see Fig. 7): first, a high amplitude narrowband waveform at 20 kHz, stable over time, generated by the inverter of a PV panel, and second, transmissions generated by PLC devices, in the form of wideband (35 kHz to 90 kHz) intermittent transmission bursts of short and variable duration (a few ms). Although one signal cannot be considered representative of the wide range of voltage distortion present in the grid, for the purpose of this paper this test signal is sufficient to show the reproducibility issues of the CISPR 16 method, as it will be illustrated in the following paragraphs.

The variations of these two waveforms over time have different characteristics. In the long-term, the emission at 20 kHz remains stable, while the PLC transmissions are short intermittent bursts. In the short-term (below 20 ms, which corresponds to the mains cycle), the emission at 20 kHz shows relevant variations in amplitude, due to the Pulse Width Modulation technique used in the inverters, as it is shown in Fig. 8.

4.4. Results

The 365 different implementations of the CISPR 16–1–1 measurement method developed in this study, all of them compliant with the standard, were applied to the test signal to calculate the QP spectra, as it is plotted in Fig. 6. Results from different implementations of the standard reflect a wide range of values. In order to quantify this dispersion and evaluate the impact of different parameters in the results, two representative frequencies were chosen: 20 kHz and 64.5 kHz, which correspond to the peaks of the disturbance generated by the PV inverter and the PLC transmissions, respectively (see Fig. 7).

The results have been grouped according to the three parameters of the CISPR 16–1–1 implementations analyzed in this paper: window function, window overlap factor and specific implementation of the QP detector. The spread of the values of each configuration at 20 kHz and 64.5 kHz is characterized by the median value and the range (difference between maximum and minimum values) in mV and in percentage with respect to the median value. The results of these calculations are shown in Table 5, where the listed parameter of the receiver implementation is fixed (common) and each row represents a specific configuration

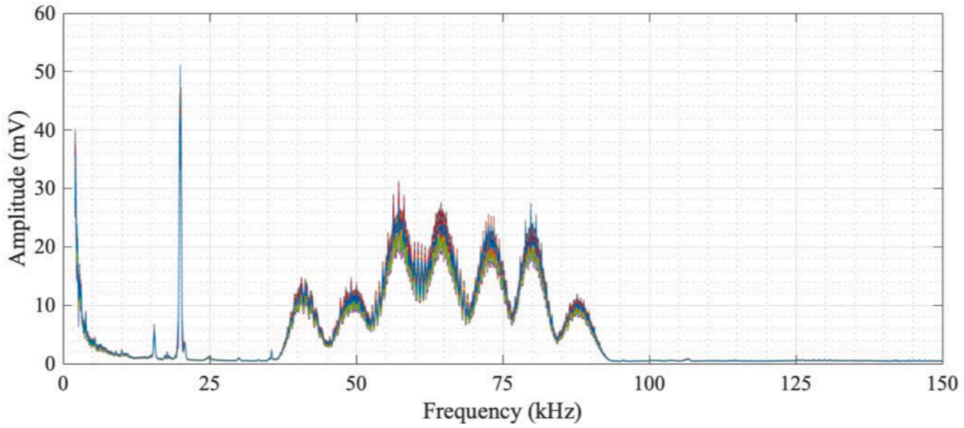

Fig. 6. Spectra of the analyzed recording obtained with the 365 compliant CISPR 16–1–1 implementations.

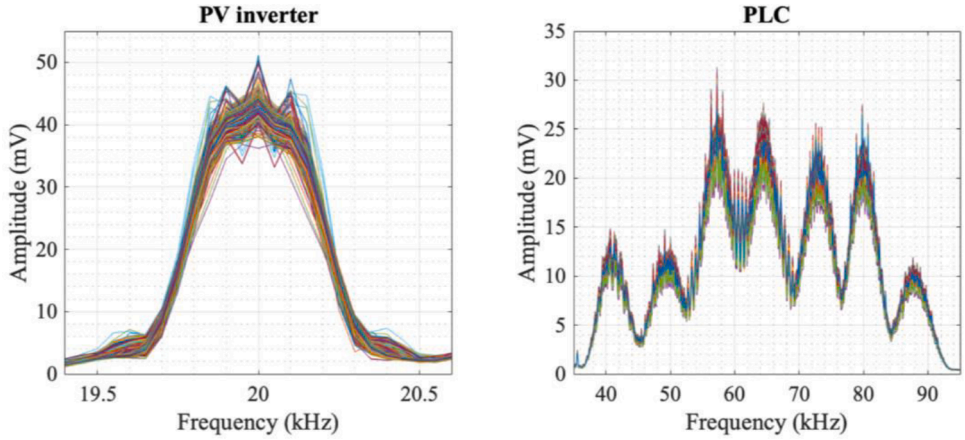

Fig. 7. Details of the emissions spectra from PV inverter and PLC devices obtained by the compliant CISPR 16–1–1 implementations.

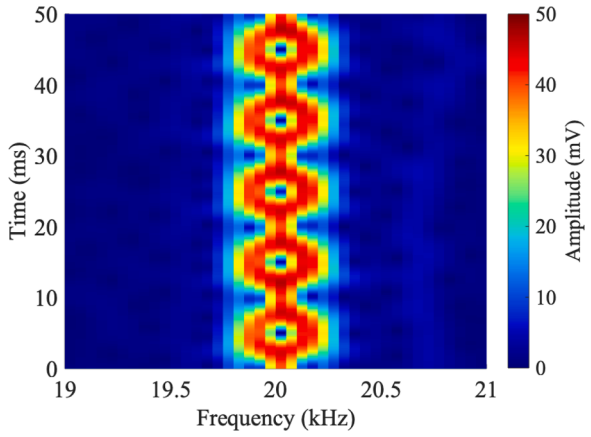

Fig. 8. Spectrogram of the test signal at 20 kHz: detail of the sub-cycle amplitude variations of the emission.

varying the rest of the parameters. For each configuration, the number of implementations that passed the calibration test and are used to calculate the range is also specified in the table. The results are also plotted in Fig. 9, in the form of scatter diagrams. In this graph, every colored point represents the output for a specific CISPR 16–1–1 implementation. In the figure, the whiskers delimit the set of results for each group, and therefore, their lengths represent the range for each configuration.

5. Analysis and discussion

5.1. Analysis of results

Results described in the previous section demonstrate that several CISPR 16–1–1 compliant implementations can be obtained, due to the wide tolerances defined in the standard. These relaxed accuracy requirements give a wide range of outputs for the same input waveform. As the QP detector takes into account the variability of the waveform over the time, the dispersion of the outputs is evaluated separately for two waveform patterns: a continuous emission in the long-term with great sub-cycle amplitude variations (20 kHz) and intermittent transmission short bursts of a PLC transmission (64.5 kHz). The spread of the outputs for these waveforms are of 34.7% and 34.3%, respectively, as it is outlined in Table 5. This wide range is considerably higher than the maximum uncertainty usually recommended for PQ grid measurements (±5%) [13]. In spite of that, all the results provided by compliant implementations of CISPR 16–1–1 are equally valid, since the specifications of the standard are met.

The effect of using different types of weighting window in the STFT can be observed in Table 5 and Fig. 9. Results are grouped in 4 different types of windows: Gaussian, General Normalized, Kaiser and Lanczos. It can be observed that the Gaussian and Kaiser windows have similar performance for both types of signals, as the median values and the amplitude range of the results are similar. This is because both window functions have similar spectral shape and, therefore, the energy they integrate in the windowing process is comparable (see Fig. 10). The

Table 5
Results.

Freq.	Parameters		Median (mV)	Range (mV)	Range (%)	No. of implem.
PV 20 kHz	Window function	Gaussian	42,5	7,8	18,5	142
		Gen. Norm.	43,5	10,2	23,5	126
		Kaiser	42,7	7,7	18,0	72
		Lanczos	48,1	7,7	16,0	25
	Overlap factor	70%	43,1	6,4	14,8	15
		75%	41,8	11,2	26,7	8
		80%	42,6	12,4	29,0	17
		85%	43,0	6,8	15,8	15
		90%	41,5	10,2	24,5	40
		95%	42,7	9,8	22,9	45
		96%	42,9	10,0	23,2	45
		97%	43,0	10,0	23,3	45
		98%	43,1	10,1	23,4	45
		99%	43,2	10,1	23,4	45
		99.5%	43,2	10,1	23,3	45
	Detector	Det. 1	42,9	11,2	26,0	156
		Det. 2	44,3	12,4	28,0	107
		Det. 3	41,7	10,8	25,9	102
	All	–	42,9	14,9	34,7	365
PLC 64.5 kHz	Window function	Gaussian	24,5	5,8	23,8	142
		Gen. Norm.	24,7	8,5	34,2	126
		Kaiser	24,5	5,8	23,5	72
		Lanczos	25,4	4,6	18,0	25
	Overlap factor	70%	24,2	2,7	11,2	15
		75%	24,2	2,2	9,0	8
		80%	23,9	6,3	26,4	17
		85%	24,8	2,6	10,5	15
		90%	24,2	4,1	16,8	40
		95%	24,5	5,0	20,2	45
		96%	24,5	4,9	20,0	45
		97%	24,6	5,0	20,4	45
		98%	24,7	5,1	20,5	45
		99%	24,8	5,1	20,6	45
		99.5%	24,8	5,1	20,6	45
	Detector	Det. 1	24,5	3,0	12,2	156
		Det. 2	26,2	5,6	21,3	107
		Det. 3	23,6	5,7	24,1	102
	All	–	24,6	8,5	34,3	365

General Normalized window provides slightly greater amplitude values and the largest dispersion of the results with respect to the rest of the windows. This effect is caused by the side lobes of this type of window, of higher magnitude compared with the rest of the windows (see Fig. 10); as a result, a greater amount of energy from adjacent frequencies is integrated and included in the Fourier analysis. Lastly, the Lanczos kernel window function provides the highest amplitude outputs. This effect is more remarkable for the PV emission, as the Lanczos window contains the widest main lobe of the selected windows (see Fig. 10), and the sub-cycle variations may be integrated in a different way.

Regarding the overlap factor between consecutive windows, the results in Table 5 and Fig. 9 show that only a limited number of implementations with overlap factors lower than 90% passes the compliance tests. In contrast, when the overlap factor is equal or higher than 95%, all the configurations considered in this work are compliant. This implies that a minimum overlap factor of 90% is recommended for the implementations to be more likely to be compliant to the standard. Results for overlap factors between 75% and 85% show lower median values, because a lower overlap factor implies that short impulses are more probable to be overlooked. Also, the sub-cycle amplitude variations of the emission at 20 kHz (see Fig. 8) are not completely covered by low overlap factors, and that is the reason why the median values are lower for these overlap factors. On the contrary, the median values of the outputs for overlap factors higher than 95% are similar (see Table 5 and Fig. 9), because these very high overlap factors ensure the proper integration of the energy of the waveform, avoiding the underestimation of short bursts of impulsive noise.

Considering that the overlap factor is directly related to the computational cost, it can be determined that overlap factors equal to or higher than 95% provide similar outputs, and therefore, 95% could be identified as an upper limit of the overlap factor. Consequently, overlap factors between 90% and 95% can be adequate to provide accurate assessment, and at the same time, avoiding inefficient extra computational cost.

The QP detector is the last aspect to be considered, in particular the mathematical basis and the specific implementation of the critically damped meter, as the response of the RC circuit is similar in all the implementations. Results show that Detector 2 provides higher outputs, mainly for PLC signals, where outputs are higher regardless of the type

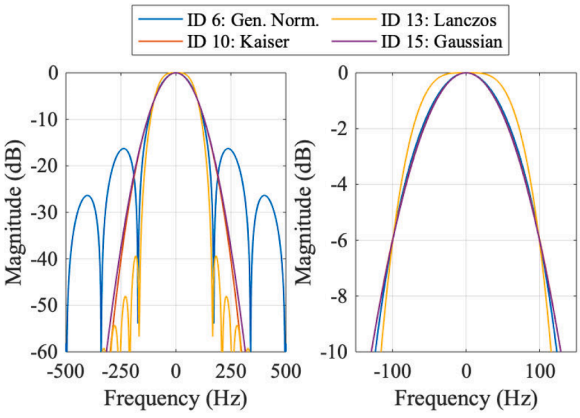

Fig. 10. Comparison of some windows selected for the analysis: (left) spectral pattern for ±500 Hz; (right) main lobe around the central frequency.

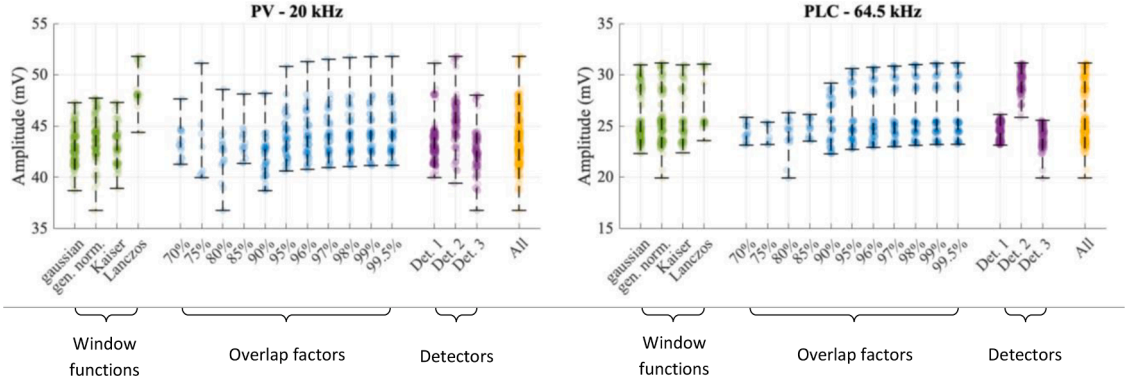

Fig. 9. Dispersion of the CISPR 16–1–1 method outputs for frequencies containing PV and PLC emissions categorized by the main parameters of the receiver.

of the window and the overlap factor (see Table 5 and Fig. 9). Additionally, Detector 1 obtains the highest number of compliant implementations, which suggests that the windowing and the overlapping have less influence in the calibration process for this detector, or that the implementation of the damped meter is better adapted to the requirements of the calibration test; moreover, it produces a lower dispersion in the outputs, mainly for the PLC transmissions. Lastly, implementations based on Detector 3 provide both the lowest number of compliant implementations and the lowest output values.

Regarding the amplitude of the outputs, it should be noticed that there is a relation between the mechanical time constant and the median value of the results. Hence, the shortest time constant (128 ms of Detector 2) provides the highest amplitude results, as the detector implementing this value reacts faster to fluctuations of the emissions. In contrast, the highest time constant (192 ms of Detector 3) provides the lowest results, due to the higher damping of fast variations, with respect to the nominal value (160 ms of Detector 1).

The divergence of the previous results is caused by two reasons: the 20% tolerance of the mechanical time constant and the technical approach (physical equations of the circuit, IIR filtering or bilinear approximation) of the implementation of the damped meter. In order to determine the impact of each factor, an additional analysis has been developed.

5.2. Response of quasi-peak detectors with same time constants

Firstly, the mechanical time constant T_{DM} is now set to the suggested value of 160 ms (see Table 4) in the three implemented detectors. Therefore, with respect to the previous analysis, T_{DM} of Detectors 2 and 3 is modified to 160 ms. This configuration is labelled as Detector 2* and 3*, to differentiate from the previous ones. The results for this configuration (see Fig. 11 and Table 6) show that the median values for each detector are somewhat closer than in the previous study case, and the spread of the outputs decreases slightly. The comparison of these results with respect to the results shown in Table 5 and Fig. 9 reveals that fixing the T_{DM} does not reduce the spread of the results noticeably, which implies that this is not a relevant factor on the dispersion of the outputs.

Secondly, to evaluate the impact of different possible techniques used to digitally implement the critically damped meter, three specific receiver configurations have been implemented and recalculated. In these configurations, the window function, the overlap factor and the time constants of the damped meter are fixed, and only the techniques to implement the damped meter digitally are different. The Lanczos window was selected since its spectral response closely matches the pre-receiver specification described in Annex A of CISPR 16–1–1, an overlap of 95% ensures that fast variations of the waveform are appropriately considered and the time constants outlined in Annex D of the standard were applied to the three implementations of the damped meters. The difference between the three implementations was the technical approach in the digital implementation of the damped meters: use of physical equations of the circuit, IIR filtering, bilinear approximation. The results (see Table 7) show that these three implementations with the same specific configuration parameters, only differing in the digital implementation of the detector provide results with differences that can exceed 5%. In the case of continuous emissions with sub-cycle variations, the range of results is 3.8%, while for the results for intermittent bursts, such as PLC transmissions, the difference is 5.6%. These differences are explained by the fact that the QP detector implementations do not follow the fluctuations of the emissions at the same rate, even though the window function, the overlap factor and the time constants are the same in all the implementations. Fig. 12 shows the evolution over time of the weighted envelopes of the QP detectors of the three implementations.

Therefore, the selection of a specific configuration does not ensure to solve the uncertainty issues of the CISPR 16–1–1 method, as the technical approach used in the implementation of the damped meter has a determinant influence on the outputs of the QP detectors.

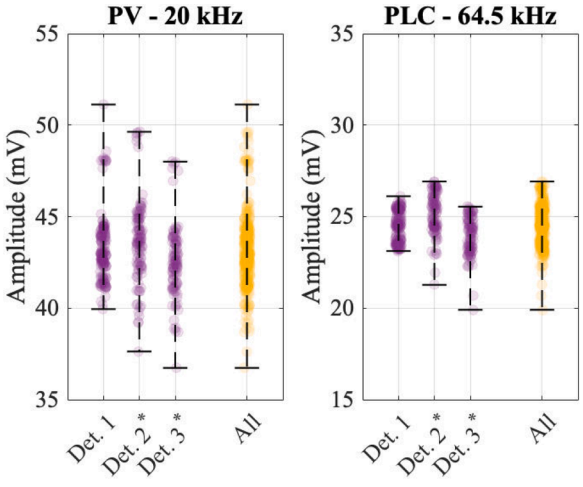

Fig. 11. Dispersion of the CISPR 16–1–1 method outputs for the same time constants of the quasi-peak detector.

Table 6
Results for the same 'TDM' value of quasi-peak detector.

Freq.	Detector	Median (mV)	Range (mV)	Range (%)	Number of implem.
PV 20 kHz	Det. 1	42,9	11,2	26,0	156
	Det. 2*	43,7	12,0	27,5	107
	Det. 3*	42,4	11,3	26,6	102
	All	43,0	14,4	33,5	365
PLC 64.5 kHz	Det. 1	24,5	3,0	12,2	156
	Det. 2*	25,4	5,6	22,3	107
	Det. 3*	24,1	5,6	23,4	102
	All	24,6	7,0	28,6	365

5.3. Discussion

The compatibility levels for conducted disturbances in LV power networks in the 9 kHz to 150 kHz range are based on quasi-peak values as defined in the CISPR 16–1–1 standard. However, no guidance about how to apply this measurement method in the grid is given. The CISPR 16 standard was defined for laboratory measurement on the basis of a super-heterodyne analogue receiver that sequentially scans the frequency range to detect worst-case emissions. Therefore, many of the specifications are defined considering the performance of analogue components, which complicates the digital implementation of the standard receiver. The 'black-box' approach of the standard, combined with high tolerances for compliance and non-normative parameters specification, lead to a wide range of compliant implementations of the CISPR 16–1–1 standard.

The wide tolerances in the definition of the window function and the compliance tests have been identified to have a great influence on the results produced by the method. The window function is defined by its frequency response, in the form of a spectral mask with wide margins

Table 7
. Results of QP detectors for a unique window and overlap.

Freq.	Detector	Quasi-peak amplitude (mV)	Median (mV)	Range (mV)	Range (%)
PV 20 kHz	Det. 1	48.1	48.1	1.8	3.8
	Det. 2*	48.8			
	Det. 3*	47.0			
PLC 64.5 kHz	Det. 1	25.4	25.4	1.4	5.6
	Det. 2*	26.2			
	Det. 3*	24.8			

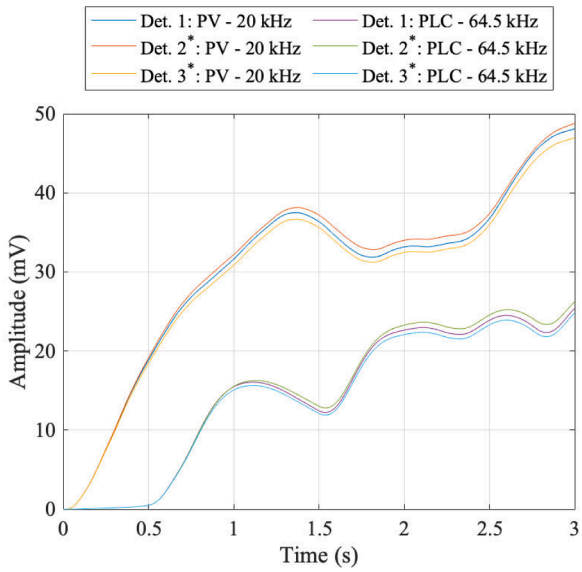

Fig. 12. Evolution of the outputs of the three quasi-peak detectors, with different design technique, for the PV emissions and the PLC transmission.

allowed in the pass-band selectivity. The mask does not define limits for the side lobes of the window function, but the amplitude of these lobes may also have a relevant influence in the results. The consequence is that a wide range of window functions of different spectral shape fulfill the mask of the standard. Moreover, the time constants defined for determining the performance of the QP detector are not normative and a deviation of 20% is allowed by the standard. The compliance tests are also defined with wide tolerances: +26% / −21% for the output when the method is applied to pure sine-waves, and an accumulated tolerance for the pulse train up to +50% / -33%. These values contrast to the accuracy usually defined for PQ measurements below 2 kHz (±5%).

The reason behind such permissive requirements can be found in the original spirit of the CISPR 16 standard series, which was developed at the beginning of the 20th century to address the need of different generations of analogue instruments and deal with the low accuracy of analogue filters. Nowadays, instruments have a much higher precision, and it is possible to achieve a better accuracy. The work presented in [29] shows how modern digital CISPR 16 receivers can achieve a far better accuracy than the standard requirements. In [29], an off-the-shelf digital CISPR 16 receiver shows an accuracy below 0.1 dB for the sine-wave test (approximately 1%) and below 0.5 dB (approximately 6%) for the response to pulses test for CISPR band C/D (up to 1 GHz). This suggests that it is technologically achievable to harmonize the 2 kHz to 150 kHz range with the accuracy requirements for PQ instruments below 2 kHz, which are in the order of 5%.

The result is that the CISPR 16 standard, when analyzing LV grid signals, allows different compliant instruments to produce a wide range of different results, all of them valid as they fulfill the standard accuracy requirements, affecting the comparability of measurements. Since there is no reference implementation, no implementation is more accurate than another, and therefore, there is no 'true' value for an input waveform linked to the standard implementation. As it has been shown, the 365 tested implementations provide a wide range of outputs for the same input waveforms, with differences up to more than 30% for real grid signals. It is remarkable that all the outputs are equally valid, as they are obtained by a CISPR 16 compliant implementation. The 365 compliant implementations of the receiver have been analyzed according to the effect of the window function, the window overlap factor and the technical approach of the QP detector on the results.

The window function selected for the Fourier analysis has a great influence on the output, mainly for waveforms with fast amplitude variations (within the mains cycle). This is because the shape of the window determines the amount and spectral content of the signal energy that is integrated for the calculations. As a result, different compliant windows extract different spectral content, providing different outputs for a specific frequency band of 200 Hz.

A high window overlap factor (> 90%) is needed to ensure that short impulses are not overlooked, but also for most of the implementations to pass the compliance test. Results show that an even higher overlap factor (> 95%) is required to obtain stable outputs. This implies that Fourier analysis must be applied periodically for very short intervals (every 1 ms for 20 ms windows), which demands larger computational effort and memory requirements for any implementation.

The QP detector is defined in the standard for analogue implementation, in terms of non-normative time constants with high tolerance, and evaluated by means of the compliance test for the whole receiver. Results show a high dependence, not only on the time constants of the receiver, but also in the technical approach used in the implementation of the digital QP detector (in this study, physical equations of the circuit, IIR filtering or bilinear approximation). This is a determinant result of this analysis, as a fixed specific configuration does not ensure that reproducibility issues are solved.

6. Conclusions

In summary, this work has investigated the suitability of the CISPR 16-1-1 measurement method for grid measurements identifying important limitations in terms of accuracy requirements and reproducibility. This in turn affects the comparability of results and might not prove suitable for grid applications and in-situ surveys. The main reason behind these limitations is due to be based on outdated specifications, and the necessity of simulating mechanical and analogue devices by means of a digital implementation.

Beside highlighting these limitations, the details of the analysis provide useful insight on potential approaches to measure quasi-peak values in LV power networks. Considering that the existing technology allows for a much better precision, one option would be to define stricter accuracy requirements for the compliance tests in CISPR 16-1-1. This has the potential of reducing the spread of results and improving the comparability of results between different instruments, while at the same time maintaining the black-box approach of the standard. An additional option would be to identify a preferential implementation i.e., a more specific definition of the parameters, namely the window function, the window overlap, and QP detector constants. This would reduce the spread of results, and the specifications could be tailored to in situ measurement requirements e.g., optimizing the computational complexity for real-time measurement. However, it would still leave room for variations due to the analogue definition of the standard, as discussed in Section 0. Moreover, it would reduce the possibility for the manufacturers to innovate their instrument design. A third option would be to define a new measurement method not based on the quasi-peak analogue detector, and then to establish a relationship between the new method's output and quasi-peak values to allow the verification of the compatibility levels in IEC 61000-2-2. Although this option would entail the effort of identifying a relationship with quasi-peak values, it would also allow for a new method to provide additional metrics to measure relevant PQ interference phenomena using, for instance, RMS values. This would be beneficial since quasi-peak values were developed to evaluate the annoyance to the human ear of a repetitive disturbance, and not to provide information on the quality of power supply.

While standardization work is still ongoing and needing evidence-based research to support decisions, this work highlights the limitations of using CISPR 16-1-1 receivers for LV networks measurements of distortion in the 9 kHz to 150 kHz region, and the need of an improved method based on modern digital calculation techniques to provide better accuracy and satisfactory reproducibility of results.

CRediT authorship contribution statement

Stefano Lodetti: Conceptualization, Methodology, Software, Investigation, Writing – original draft. **Alexander Gallarreta:** Software, Formal analysis, Investigation, Writing – original draft. **Deborah Ritzmann:** Formal analysis, Writing – review & editing. **Victor Khokhlov:** Validation. **Paul Wright:** Project administration, Funding acquisition. **Jan Meyer:** Supervision. **Igor Fernández:** Formal analysis, Investigation. **David de la Vega:** Supervision, Writing – review & editing, Funding acquisition.

Declaration of Competing Interest

The authors declare that they have no known competing financial interests or personal relationships that could have appeared to influence the work reported in this paper.

Data availability

No data was used for the research described in the article.

Acknowledgements

The authors express their gratitude to Dimitrij Klingbeil and Michael Schwenke of Siemens AG for sharing one of the digital implementations of the CISPR 16–1–1 standard analyzed in this work.

References

[1] S.K. Rönnberg, et al., On waveform distortion in the frequency range of 2kHz-150kHz - review and research challenges, Electr. Power Syst. Res. 150 (2017).
[2] I. Fernandez, N. Uribe-Pérez, I. Eizmendi, I. Angulo, D. de la Vega, A. Arrinda, T. Arzuaga, Characterization of non-intentional emissions from distributed energy resources up to 500 kHz: a case study in Spain, Int. J. Electric. Power & Energy Syst. 105 (2019) 549–563.
[3] J. Sutaria, S. Rönnberg, Á. Espín-Delgado, Analysis of supraharmonics in a three-phase frame, Electr. Power Syst. Res. 203 (2022).
[4] Á. Espín-Delgado, S. Rönnberg, T. Busatto, V. Ravindran, Bollen M, Summation law for supraharmonic currents (2–150kHz) in low-voltage installations", Electr. Power Syst. Res. 184 (2020).
[5] J. Meyer, V. Khokhlov, C. Waniek, and T. Wohlfahrt, "Overview and classification of interferences in the frequency range 2-150kHz (Supraharmonics),"in 2018 International Symposium on Power Electronics, Electrical Drives, Automation and Motion, pp. 165–170, 2018.
[6] F. Zavoda, M.H. Bollen, and S.K. Rönnberg, "CIGRE/CIRED JWG C4.24, Power Quality and EMC Issues associated with future electricity networks: status report," in In CIGRE Sessions, Paris, 2016.
[7] CENELEC SC 205A, CLC/TR 50669, Investigation Results on Electromagnetic Interference in the Frequency Range below 150kHz. 2017.
[8] N. Uribe-Pérez, I. Angulo, L. Hernández-Callejo, T. Arzuaga, D. de la Vega, A. Arrinda, Study of unwanted emissions in the CENELEC - A band generated by distributed energy resources and their influence over narrow band power line communications, Energies 9 (12) (2016), 1007.
[9] D. Ritzmann, S. Lodetti, D. de la Vega, V. Khokhlov, A. Gallarreta, P. Wright, J. Meyer, I. Fernández, D. Klingbeil, Comparison of measurement methods for 2–150kHz conducted emissions in power networks, IEEE Trans. Instrumentation and Measurement 70 (2021) 1–10.
[10] T.M. Mendes, C.A. Duque, L.R. Manso da Silva, D.D. Ferreira, J. Meyer, P. R. Ribeiro, Comparative analysis of the measurement methods for the supraharmonic range, Int. J. Electric. Power & Energy Syst. 118 (2020).
[11] V. Khokhlov, J. Meyer, A. Grevener, T. Busatto, S.K. Rönnberg, Comparison of measurement methods for the frequency range 2-150kHz (Supraharmonics) based on the present standards framework, IEEE Access (2020).
[12] International Electrotechnical Commission, "Electromagnetic compatibility (EMC) - Part 4-30: Testing and measurement techniques - Power quality measurement methods," *IEC 61000-4- 30 Ed.3*, 2015.
[13] International Electrotechnical Commission, "Electromagnetic compatibility (EMC) - Part 4-7: Testing and measurement techniques - General guide on harmonics and interharmonics measurements and instrumentation, for power supply systems and equipment connected thereto," *IEC 61000-4-7:2002+AMD1*:2008.
[14] International Electrotechnical Commission, Specification for radio disturbance and immunity measuring apparatus and methods - Part 1-1: radio disturbance and immunity measuring apparatus - measuring apparatus, CISPR 16-1-1 (2019).
[15] International Electrotechnical Commission, "CISPR 16-2-1:2014. Specification for radio disturbance and immunity measuring apparatus and methods - Part 2-1: Methods of measurement of disturbances and immunity - Conducted disturbance measurements", 2014.
[16] International Electrotechnical Commission, "IEC 61000-2-2:2002 + AMD1:2017 + AMD2: 2018. Electromagnetic compatibility (EMC) - Compatibility levels for low-frequency conducted disturbances and signaling in public low-voltage power supply systems".
[17] C. Keller and K. Feser, "Fast emission measurement in time domain," in *14th International Zurich Symposium and Technical Exhibition on Electromagnetic Compatibility*. Zurich, Switzerland: Communication Technology Laboratory of the Swiss Federal Institute of Technology Zurich, 2001.
[18] F. Krug and P. Russer, "Ultra-fast broadband EMI measurement in time- domain using FFT and periodogram", in *IEEE International Symposium on Electromagnetic Compatibility*, 2002.
[19] International Electrotechnical Commision, "CISPR/TR 16- 3:2010+A1:2012. Specification for radio disturbance and immunity measuring apparatus and methods - Part 3: CISPR technical reports", 2015.
[20] F. Krug, P. Russer, Quasi-peak detector model for a time-domain measurement system, IEEE Trans. Electromagnetic Compatibility 47 (2) (2005) 320–326.
[21] M.A. Azpurua, M. Pous, F. Silva, Specifying the waveforms for the calibration of CISPR 16-1-1 measuring receivers, IEEE Trans. Electromagnetic Compatibility (2019) 01–09.
[22] M.A. Azpurua, M. Pous, J.A. Oliva, B. Pinter, M. Hudlicka, F. Silva, Waveform approach for assessing conformity of CISPR 16-1-1 measuring receivers, IEEE Trans. Instrumentation and Measurement 67 (5) (2018).
[23] L. Sandrolini, A. Mariscotti, Impact of short-time fourier transform parameters on the accuracy of EMI spectra estimates in the 2-150kHz supraharmonic interval, Electr. Power Syst. Res. 195 (March 2021).
[24] M. Schwenke and D. Klingbeil, "Application aspects and measurement methods in the frequency range from 9kHz to 150kHz," in *Proc. 25th International Conference on Electricity Distribution (CIRED)*, Madrid, Spain, 2019.
[25] V. Khokhlov, J. Meyer, A. Grevener, T. Busatto, S.K. Rönnberg, Comparison of measurement methods for the frequency range 2- 150kHz (Supraharmonics) based on the present standards framework, IEEE Access (2020).
[26] I. Fernández, D. de la Vega, A. Arrinda, I. Angulo, N. Uribe-Pérez, A. Llano, Field trials for the characterization of non-intentional emissions at low-voltage grid in the frequency range assigned to NB-PLC technologies, Electronics (Basel) 8 (2019).
[27] S. Braun, A. Frech, and P. Russer, "CISPR specification and measurement uncertainty of the time-domain EMI measurement system," in *IEEE International Symposium on Electromagnetic Compatibility*. Detroit, USA, 2008.
[28] M. Monti, E. Puri, and M. Monti, "Hidden aspects in CISPR 16-1-1 full compliant fast fourier transform EMI receivers," in *2016 IEEE International Symposium on Electromagnetic Compatibility - EMC EUROPE*, 2016.
[29] Medler, J., Uncertainty contribution of the EMI Test Receiver in RF disturbance measurements. *2010 Asia-Pacific Symposium on Electromagnetic Compatibility, APEMC 2010*, 994–997. 2010.